Quantifying the tropospheric ozone radiative effect and its temporal evolution in the satellite-era

Richard J. Pope[1,2], Alexandru Rap[1], Matilda A. Pimlott[1], Brice Barret[3], Eric Le Flochmoen[3], Brian J. Kerridge[4,5], Richard Siddans[4,5], Barry G. Latter[4,5], Lucy J. Ventress[4,5], Anne Boynard[6,7], Christian Retscher[8], Wuhu Feng[1,9], Richard Rigby[1,10], Sandip S. Dhomse[1,2], Catherine Wespes[11] and Martyn P. Chipperfield[1,2]

1: School of Earth and Environment, University of Leeds, Leeds, UK

2: National Centre for Earth Observation, University of Leeds, Leeds, UK

3: LAERO/OMP, Université de Toulouse, Toulouse, France

4: Remote Sensing Group, STFC Rutherford Appleton Laboratory, Chilton, UK

5: National Centre for Earth Observation, STFC Rutherford Appleton Laboratory, Chilton, UK

6: LATMOS/IPSL, Sorbonne Université, UVSQ, CNRS, Paris, 75005, France

7: SPASCIA, Ramonville-Saint-Agne, 31520, France

8: ESA/ESRIN, Frascati, Italy

9: National Centre for Atmospheric Science, University of Leeds, Leeds, UK

10: Centre for Environmental Modelling and Computation, University of Leeds, Leeds, UK

11: Université libre de Bruxelles (ULB), Spectroscopy, Quantum Chemistry and Atmospheric Remote Sensing, Brussels, Belgium

Submitted to *Atmospheric Chemistry and Physics*

Correspondence to: Richard J. Pope (r.j.pope@leeds.ac.uk)

Key Points:

- Using satellite data and model simulations, we quantify ~~the long-term~~decadal (2008-2017) global average tropospheric ozone radiative effect (TO$_3$RE) to range between 1.21 and 1.~~28~~ 26 W/m^2.
- Satellite/modelled decadal (2008-2017) ~~long-term~~ trends in the tropospheric ozone radiative effect ~~have remained stable~~show negligible change with time. ~~(2008-2017) yielding no substantial changing influences on climate.~~
- This TO$_3$RE negligible trend is caused by competing processes (meteorological variability and temporal changes in precursor emissions) over the decade.
- ~~Meteorological variability has been important in stabilising the global tropospheric ozone radiative effect with time.~~

Abstract:

Using state-of-the-art satellite ozone profile products, and chemical transport model, we provide an updated estimate of the tropospheric ozone radiative effect (TO$_3$RE) and observational constraint on its variability over the decade 2008-2017. Previous studies have shown the short-term (i.e. a few

Formatted: Space After: 6 pt

Formatted: Font: Bold

years) globally weighted average TO_3RE to be 1.17±0.03 W/m^2. However, from our analysis, using decadal (2008-2017) ozone profile datasets from the Infrared Atmospheric Sounding Interferometer, average TO_3RE ranges between 1.21 and 1.26 W/m^2. Previous studies have shown the short-term (i.e. a few years) globally weighted average TO_3RE to be 1.17±0.03 W/m^2, while our analysis suggests that the long-term (2008-2017) average TO_3RE to be 1.21-1.28 W/m^2. Over this decade, the modelled/observational TO_3RE linear trends show negligible change (i.e. ±0.1%/year), so the tropospheric ozone radiative contribution to climate has remained stable with time. Two model sensitivity experiments fixing emissions and meteorology to one yearone-year (i.e. start year – 2008) show that that temporal changes in ozone precursor emissions (increasing contribution) and (meteorological factors (decreasing contribution) have counteracting tendencies have had limited (substantial) impacts on the long-termleading to a negligible tendency of globally weighted average TO_3RE tendency. Here, the meteorological variability in the tropical/sub-tropical upper troposphere is dampening any tendency in TO_3RE from other factors (e.g. emissions, atmospheric chemistry).

Plain Language Summary:

Tropospheric ozone is a potent air pollutant and an important short-lived climate forcer (SLCF). It is a secondary pollutant formed through chemical reactions of precursor gases and sunlight. As a SLCF, it influences both the incoming solar short-wave radiation and the outgoing long-wave radiation throughout the troposphere but has the largest radiative impact in the upper troposphere where the balance between the two yields a net positive (i.e. warming) effect at the surface. As a SLCF, it influences the incoming solar short-wave radiation and the outgoing long-wave radiation in the upper troposphere (approximately at altitudes of 10-15 km) where the balance between the two yields a net positive (i.e. warming) effect at the surface. The majority of previous estimates of the tropospheric ozone radiative effect (TO_3RE) have been quantified from atmospheric chemistry climate model simulations. However, satellite retrievals of tropospheric ozone now have decadal records and provide the opportunity to quantify the TO_3RE and complement estimates based on model simulations. However, satellite retrievals of tropospheric ozone in recent decades have provided the opportunity to estimate these model TO_3RE estimates. In this study, we utilise satellite ozone profile retrievals from the Infrared Atmospheric Sounding Interferometer (IASI), on-board the MetOp-A satellite, to derive a long-termdecadal average TO_3RE estimate of 1.21-1.28 26W/m^2. While this builds upon previous studies (e.g. TO_3RE estimates of 1.17±0.03 W/m^2), the improved spatial coverage and temporal record of IASI also allows for the assessment of TO_3RE variability and tendencies on a decadal scale. Here, we find negligible trends in the TO_3RE (2008-2017) suggesting that the decadal contribution of tropospheric ozone to climate, via radiative properties, remained stable over that period. has been limited.

1. Introduction

Tropospheric ozone (TO_3) is a short-lived climate forcer (SLCF; Forster et al., 2021; Szopa et al., 2021). It is the third most important greenhouse gas (GHG; Forster et al., 2021; Myhre et al., 2013) and a hazardous air pollutant with adverse impacts on human health (WHO, 2018; Fleming et al., 2018) and the biosphere (e.g. agricultural and natural vegetation; Mills et al., 2018; Sitch et al., 2007). Since the pre-industrial (PI) period, anthropogenic activities have increased the atmospheric loading of ozone (O_3) precursor gases, most notably nitrogen oxides (NO_x) and methane (CH_4), resulting in an increase in TO_3 of 25-50% since 1900 (Gauss et al., 2006; Lamarque et al., 2010; Szopa et al., 2021; Young et al., 2013). More recently, since the mid-twentieth century, northern hemispheric TO_3 has increased by 30-70%. The PI to present day (PD) radiative forcing (RF) from TO_3 is estimated by the Intergovernmental Panel on Climate Change (IPCC) to be 0.47 W m^{-2} (Forster et al., 2021) with an uncertainty range of 0.24–0.70 W m^{-2}.Tropospheric ozone (TO_3) is a short-lived climate forcer (SLCF). It is the third most important greenhouse gas (GHG; Myhre et al., 2013) and a hazardous air pollutant with adverse impacts on human health (WHO, 2018) and the biosphere (e.g. agricultural and natural vegetation; Sitch et al., 2007). Since the pre-industrial (PI) period, anthropogenic activities have increased the atmospheric loading of ozone (O_3) precursor gases, most notably nitrogen oxides (NO_x) and methane (CH_4), resulting in an increase in TO_3 of 25-50% since 1900 (Gauss et al., 2006; Lamarque et al., 2010; Young et al., 2013). The PI to present day (PD) radiative forcing (RF) from TO_3 is estimated to be 0.4 (0.2-0.6) Wm^{-2} (Myhre et al., 2013; Stevenson et al., 2013) based on model simulations.

While models provide a valuable framework to quantify the TO_3 RF, observations are required to validate the models' representation of TO_3 and TO_3 RF. Observations are not available for the PI, but multiple satellite products of TO_3 are readily available in the PD (e.g. Richards et al., 2008; Boynard et al., 2018; Barret et al., 2020). The tropospheric ozone radiative effect (TO_3RE) is defined as the radiative flux imbalance at the tropopause between incoming short-wave solar radiation and the outgoing long-wave radiation due to the presence of TO_3 (Rap et al., 2015). Therefore, satellite ozone profile datasets from infrared instruments, in combination with off-line ozone radiative kernels (e.g. Bowman et al., 2013; Rap et al., 2015), can be used to quantify the PD TO_3RE. This can then either constrain model estimates of PD TO_3RE or be used directly with modelled PI TO_3RE to derive the TO_3RF.Therefore, satellite ozone profile datasets from infrared instruments, in combination with off-line ozone radiative kernels to account for vertical sensitivity (e.g. Bowman et al., (2013); Rap et al., 2015), can be used to quantify the PD TO_3RE and thus provide some constraint on modelled TO_3RE which is used to derive the TO_3RF.

Several studies have previously used satellite data to derive short-term estimates of the TO_3RE (i.e. from a few months of data). Joiner et al., (2009) used tropospheric column ozone (TCO_3) data based on two satellite instruments: Ozone Monitoring Instrument (OMI) and Microwave Limb Sounder (MLS) measurements, also known as OMI-MLS product for January and July 2005, to estimate the resultant instantaneous TO_3RE at the tropopause to be 1.53 W/m^2. Worden et al., (2008) used ozone profile data for 2006 from the Tropospheric Emissions Spectrometer (TES), on-board NASA's Aura satellite, to estimate the average instantaneous long-wave TO_3RE at the top-of-the-atmosphere (TOA) over the oceans (45°S-45°N) to be 0.48±0.14 W/m^2. Worden et al., (2011), using TES data for August 2006, estimated the instantaneous long-wave TO_3RE at TOA to be 0.33 W/m^2. Later, Bowman et al., (2013) also used TES data (averaged between 2005 and 2009) to constrain the simulated instantaneous long-wave TO_3RE from an ensemble model average. They found that seasonally, TES long-wave TO_3RE peaks in northern Africa/Mediterranean/Middle East in June-July-August over 1.0 W/m^2 with minimum values (0.0-0.2 W/m^2) over the winter-time high-latitudes. Overall, the ensemble average long-wave TO_3RE low bias was 0.12 W/m^2. Doniki et al., (2015) took this further by calculating the instantaneous long-wave TO_3RE from the Infrared Atmospheric Sounding Interferometer (IASI), though using a small subset of the data, and found estimates from Worden et al., (2008), using TES, had a low bias of ~25%. Rap et al., (2015) also used TES satellite ozone profile observations (2005-2008) in combination with the -TOMCAT chemical transport model (CTM) and provided the first robust satellite constraint on annual globally weighted resultant TO_3RE (after stratospheric temperature adjustment) with a range of 1.17±0.03 W/m^2.

Following the methodology adopted in Rap et al. (2015), we exploit satellite ozone profile data from IASI, on the MetOp-A satellite, which has a longer-term record and considerably denser spatial coverage than TES, in combination with the TOMCAT CTM, to improve the TO_3RE estimate and provide the first quantification of its decadal variability. ~~Following the methodology adopted in Rap et al. (2015), we exploit satellite ozone profile data from IASI, on the MetOp-A satellite, which has a long-term record and substantial spatial coverage, in combination with the TOMCT CTM, to improve the TO_3RE estimate and investigate its long-term variability and implications for climate.~~ The satellite data, radiation model and CTM used are discussed in Section 2, our results are presented in Section 3 and Section 4 summarises our conclusions.

2. Observations and Model

2.1. Satellite Observations

IASI is a Michelson interferometer with a nadir-viewing spectral range between 645 and 2760 cm^{-1} with spectral sampling of 0.25 cm^{-1} (Illingworth et al., 2011). It measures simultaneously in four fields of view (FOV, each circular at nadir with a diameter of 12 km) in a 50 x 50km square which are scanned across track to sample a 2200 km-wide swath (Clerbaux et al., 2009). IASI, on Eumetsat's MetOp-A satellite, is in a sun-synchronous polar orbit with equator crossing local times of 9.30 (day) and 21.30 (night).

The three IASI products we use in this study are the IASI-FORLI product (vn 20151001, IASI-FORLI, 2020; Boynard et al., 2018; Wespes et al., 2018), the IASI-SOFRID product (vn 3.5, IASI-SOFRID, 2022; Barret et al., 2020) and the RAL IASI-IMS product (IASI-IMS, 2022; Pope et al., 2021; Pimlott et al. ,2022) between 2008 and 2017 (i.e. period of consistent data coverage for all the IASI products). All three products use an optimal estimation method (OEM, Rogers, 2000) to retrieve ozone. Both IASI-SOFRID and IASI-IMS use the RTTOV radiative transfer model (Saunders et al. 1999), while the IASI-FORLI product uses look-up tables to speed up its radiative transfer calculations (Hurtmans et al., 2012). Meteorological inputs (pressure, water vapour, temperature and clouds) for IASI-FORLI come from Eumetsat level-2 data, while IASI-SOFRID uses ECMWF operational analyses and IASI-IMS uses ECMWF surface pressures and co-retrieves other meteorological and surface variables. For the ozone apriori, IASI-FORLI and IASI-IMS use the ozone climatology of McPeters et al., (2007), while IASI-SOFRID uses the dynamical ozone climatology described in Sofieva et al., (2014).

The IASI-FORLI level-2 data are filtered for a geometric cloud fraction <0.2, degrees of freedom > 2.0, O_3 values > 0.0, solar zenith angle < 80.0° and the surface to 450 hPa sub-column O_3 / total column O_3 < 0.085. The IASI-SOFRID data were provided on a 1.0°×1.0° horizontal grid (i.e. level-3 product, but daily temporal resolution – we used daytime retrievals only) with filtering already applied as in Barret et al., (2020). Here, only O_3 values > 0.0 were used. For IASI-IMS level-2, the data are filtered for a geometric cloud fraction <0.5, O_3 values > 0.0, solar zenith angle < 80.0° and a cost function < 1000.0. However, for IASI-IMS, we relaxed the geometric cloud fraction threshold to 0.5 as it retains more data as the data product in this study has only been processed for 1 in 10 days and 1 in 4 pixels.

Overall, IASI provides substantially denser spatial sampling and a longer-term record than its predecessor instruments. For instance, TES provided homogenous global coverage, albeit with sparse spatial sampling, every 16 days (Rap et al., 2013) over a 6-year period (2005-2010), while IASI on MetOp-A provided comparatively dense global coverage twice per day between 2008 and 2020 (though we focus on 2008-20217 where the IASI products have consistent records). Thus, making it suitable to investigate decadal average spatial patterns in TO_3RE and decadal scale interannual variability.

2.2. Ozonesondes

Despite the three IASI ozone profile products using the same radiance data, the three retrieval schemes produced systematic differences between the products in the long-term TCO_3 average (e.g. **Figures S2 and S3** from the **Supporting Information (SI)**). Though, the spatial structure in the three products compares well. Therefore, to harmonise the three IASI TCO_3 data sets (i.e. absolute values but not long-term variability) we use ozonesonde data from the World Ozone and Ultraviolet Radiation Data Centre (WOUDC; WOUDC, 2023), the Southern Hemisphere ADditional Ozonesondes (SHADOZ; SHADOZ, 2023) project and the Global Monitoring Laboratory, National Oceanic and Atmospheric Administration (NOAA; NOAA, 2023). Here, O_3 measurements were rejected if the O_3 or pressure values were unphysical (i.e. < 0.0), if the O_3 partial pressure > 2000.0 mPa or the O_3 value was set to 99.9, and whole ozonesonde profiles were rejected if least 50% of the measurements did not meet these criteria. These criteria are similar to those applied by Keppins et al., (2018) and Hubert et al., (2016). To allow for direct like-for-like comparisons between the two quantities, accounting for the vertical sensitivity of the satellite, the instrument averaging kernels (AKs) are applied the ozonesonde profiles as:

$$\boldsymbol{sonde_{AK}} = \boldsymbol{AK}.(\boldsymbol{sonde_{int}} - \boldsymbol{apr}) + \boldsymbol{apr} \qquad (1)$$

where $\boldsymbol{sonde_{AK}}$ is the modified ozonesonde sub-column profile, $\boldsymbol{AK}$ is the averaging kernel matrix, $\boldsymbol{sonde_{int}}$ is the ozonesonde sub-column profile interpolated on the satellite pressure grid and $\boldsymbol{apr}$ is the a priori for the satellite retrieval. For the application of the AKs to the ozonesonde profiles, the full ozone profile is required which is not available from the ozonesondes (i.e. mid-stratosphere and above). Therefore, the ozonesonde profile above its minimum pressure level is extended using the apriori profile from the corresponding satellite product. The profile is smoothed vertically across the joining pressure level to avoid a profile discontinuity.

Once the ozonesondes had been co-located with the satellite data (i.e. within 6-hours and 500 km) and the AKs applied, the two datasets were compared across the full 2008-2017 period. We typically find a global annual TCO_3 systematic bias of 14.9%, 2.7% and 17.4% for IASI-FORLI, IASI-SOFRID and IASI-IMS, respectively, which is consistent with Boynard et al., (2018), Barret et al., (2020) and Pimlott et al., (2022). Here, we generated annual-latitude (30° bins) bias correction factors (BCF) which were applied to the gridded satellite records (**see SI-2**) to harmonise the retrieved TCO_3 (i.e. remove the systematic errors) and scale the derived TO_3RE. This is an important exercise as it provides a more accurate absolute range in satellite retrieved TCO_3 (and the ozone values used to derive the TO_3RE) but as the ozonesondes generally have poor spatial coverage, the global coverage and spatial distribution of the satellite data is critical in our analysis. Note, that as a climatology was used, the systematic biases in the satellite records were affected but their long-term temporal variability retained.

2.3. TOMCAT

In this study, we use the 3D global chemical transport model TOMCAT (Chipperfield, 2006), which has a detailed tropospheric chemistry scheme including 229 gas-phase reactions and 82 advected tracers (Monks et al., 2017). Model heterogeneous chemistry uses size-resolved aerosol from the

GLOMAP module (Mann et al., 2010). The model was run between 2008 and 2017 at a 2.8°×2.8° spatial resolution with 31 vertical levels between the surface and 10hPa. Here, climatological fields of trace gases/aerosols are used as the vertical boundary conditions (including stratospheric ozone). ~~.~~ The model is forced by meteorological reanalyses (ERA-Interim) from the European Centre for Medium-Range Weather Forecasts (ECMWF; Dee et al., 2011) including reanalysis cloud fields and mass fluxes (e.g. as in Rowlinson et al., 2020, Pimlott et al., 2022). Annually varying anthropogenic emissions come from the Coupled Model Intercomparison Project Phase 6 (CMIP6, Feng et al., 2020). Climatological biogenic emissions are from the Chemistry-Climate Model Initiative (CCMI; Morgenstern et al., 2017) but isoprene and monoterpene emissions are annually varying from the Joint UK Land Environment Simulator (JULES, Pacifico et al., 2011) within the free-running UK Earth System Model (UKESM Sellar et al., 2019) from a CMIP6 historical setup ~~within the free-running UK Earth System Model (UKESM, Sellar et al., 2019)~~. Other natural emissions come from the Precursors of Ozone and their Effects in the Troposphere (POET, Olivier et al., 2003) and biomass burning emissions from the Global Fire Emissions Database (GFED) version 4 (van der Werf et al., 2017). For methane (CH_4), the model tracer is scaled to the annually varying global averaged surface CH_4 value from NOAA (Dlugokencky, 2020). The model was spun up for 1-year (2007) and the model tracers output daily at 09:30 local time (LT) globally to match the MetOp-A daytime overpass time. When comparing with IASI, the satellite AKs are applied to the TOMCAT vertical ozone profiles in the same way as the ozonesondes (i.e. **Equation 1**). Here, the TOMCAT ozone profile (already temporally co-located) is co-located from the model grid box the retrieval sits in. To investigate the importance of emissions and meteorology on TO_3 and TO_3RE, two sensitivity experiments were run between 2008 and 2017 using repeating emissions and meteorology for 2008 (i.e. start of the time-series) annually in the model simulation over the time period.

2.4. Radiative Transfer Model and Kernel

The TO_3RE was calculated using a radiative kernel, derived from the SOCRATES off-line radiative transfer model (Edwards and Slingo, 1996), in combination with TOMCAT and the three IASI ozone products. ~~The TO_3RE was calculated using the SOCRATES off-line radiative transfer model (Edwards and Slingo, 1996) in combination with TOMCAT and the three IASI ozone products.~~ SOCRATES has six bands in the short-wave and nine in the long-wave. Meteorological inputs (temperature, water vapour, surface albedo) into SOCRATES to derive the radiative kernel are based on climatological ECMWF ERA-Interim reanalysis. Cloud fields are based on 2000 data from International Satellite Cloud Climatology Project data (Rossow and Schiffer, 1999), while aerosols have been ignored. To account for stratospheric temperature adjustments, Rap et al., (2015) used the dynamical heating approximation (Fels et al., 1980). This involved accounting for changes in the stratospheric heating rate determined from the model due to the O_3 perturbation, which were applied to the temperature field, with the model run iteratively until stratospheric temperatures reached equilibrium (Rap et al., 2015). This approach of using the SOCRATES off-line radiative kernel with output from model simulations to derive the TO_3 radiative effect has been used in several studies e.g. Rap et al., (2015), Scott et al., (2018), Iglesias-Suarez et al. (2018) and Rowlinson et al., (2020).

To derive the satellite TO_3RE, the annual average IASI 3D ozone field is multiplied by the off-line radiative kernel (grid box by grid box) and then summed from the surface to the tropopause pressure. Here, the IASI ozone data is mapped onto the spatial resolution of the radiative kernel and then interpolated vertically onto its pressure grid. The equation for each grid box is:

$$TO_3RE = \sum_{i=surf}^{trop} RK_i \times O_{3i} \times dp_i/100 \qquad (2)$$

where *TO_3RE* is the tropospheric ozone radiative effect (W/m^2), *RK* is the radiative kernel (W/m^2/ppbv/100 hPa), *O_3* is the satellite ozone grid box value (ppbv), *dp* is the pressure difference between vertical levels (hPa) and *i* is the grid box index between the surface pressure level and the tropopause pressure. The tropopause pressure is based on the World Meteorological Organisation (WMO) definition of "the lowest level at which the temperature lapse rate decreases to 2 K/km or less" (~~Bethan et al., 1996~~WMO, 1957).

3. Results

3.1. Tropospheric Ozone Radiative Effect

Figure 1 shows the IASI derived TCO_3, TO_3RE and normalised TO_3RE (NTO_3RE, i.e. the TO_3RE divided by its TCO_3 as in Rap et al., (2015)). For the TCO_3, the three harmonised IASI products have good spatial agreement in the decadal (2008-2017) average, with a background north-south hemisphere gradient of approximately 30.0-40.0 to 15.0-25.0 DU. Peak TCO_3 (>40.0 DU) occurs over East Asia, the Middle East and in ozone outflow from central Africa (e.g. production from lightning and biomass burning precursor gases (Moxim & Levy, 2000)). The global average TCO_3 values for IASI-FORLI, IASI-SOFRID and IASI-IMS are 32.6 DU, 29.9 DU and 29.9 DU, respectively (**Figure 1 left column** and **Table 1**). From **Table 1**, degrees of freedom of signal (DOFS) are approximately 1.0 for the troposphere (i.e. $DOFS_{trop}$) and also in the upper troposphere – lower stratosphere (UTLS, $DOFS_{utls}$) – i.e. the vertical region where the O_3 radiative effect is most prominent). These DOFS are derived on a global scale using IASI data for 2008. They show there to be sufficient information in the troposphere from IASI to derive radiative effect metrics. Therefore, like in Rap et al., (2015), we are confident in our approach to directly use the satellite data to derive the observational TO_3RE.

When the TO_3RE is calculated (**Figure 1 middle column**), peak values occur over the sub-tropics, Africa and Australia ranging consistently between approximately 2.0 and 2.5 W/m^2 for each IASI product. The minimum values are found at high latitudes ranging between 0.0 and 0.8 W/m^2. The bottom panel of **Figure 1** shows the zonally average profiles weighted by the cosine of latitude (similar to Rap et al., 2015). This accounts for area weighting in the derived TO_3RE for different latitude bands on the global weighted average. Here, TCO_3 is near-zero at high-latitudes, approximately 15.0-20.0 DU at mid-latitudes, peaking at 28.0-33.0 DU in the sub-tropics and then decreasing by several DU in the tropics. The corresponding TO_3RE profiles follow a similar pattern with near-zero values at high-latitudes, approximately 0.5-1.0 W/m^2 at mid-latitudes, peaking at 1.5 W/m^2 in the sub-tropics and then decreasing to 1.1-1.2 W/m^2 in the tropics. Therefore, the sub-tropics have the largest contribution to the global TO_3RE. The global weighted TO_3RE averages for IASI-FORLI, IASI-SOFRID and IASI-IMS are 1.23, 1.21 and 1.21 W/m^2, respectively (**Figure 1** and **Table 1**).

The NTO_3RE (**Figure 1 right column**) provides an estimate of where the TO_3RE is most sensitive to changes in TCO_3 (i.e. the unit of TO_3RE per unit of TCO_3). Peak NTO_3RE (>50.0 mW/m^2/DU) occurs at similar locations to the peak TO_3RE (e.g. Africa and Australia), while the minimum values (10.0-20.0 mW/m^2/DU) occur at high-latitudes. Over the sub-tropical oceans, there are NTO_3RE values of similar magnitude (approximately 45.0 mW/m^2/DU). Therefore, despite some regions having lower TCO_3 and TO_3RE values (e.g. the South Pacific vs. the South Atlantic and Indian Ocean), the sensitivity to ozone perturbations (i.e. radiative effect per unit of TO_3) is similar in these regions.

Formatted: Outline numbered + Level: 1 + Numbering Style: 1, 2, 3, … + Start at: 1 + Alignment: Left + Aligned at: 0.63 cm + Indent at: 1.27 cm

Formatted: Indent: Left: 0.63 cm, Outline numbered + Level: 2 + Numbering Style: 1, 2, 3, … + Start at: 1 + Alignment: Left + Aligned at: 0.63 cm + Indent at: 1.9 cm

Overall, the global weighted average NTO_3RE is 37.78, 40.43 and 40.60 mW/m^2/DU for IASI-FORLI, IASI-SOFRID and IASI-IMS, respectively. It is likely that differences between the three ozone retrieval schemes could be causing the differences between globally averaged NTO_3RE values. As the IASI-FORLI NTO_3RE is lower, while having the highest global average TCO_3 and TO_3RE, it suggests that IASI-FORLI has a larger fraction of TO_3 is located in the mid-troposphere, where the radiative kernel has less sensitivity than the upper troposphere. Further to this, as the IASI ozone products only have approximately 1.0 DOFS in the troposphere (**Table 1**), the harmonisation of the products using the ozonesondes can best be done on a tropospheric column level. As a result, the scaling of the satellite derived TO_3RE is done based on the relationship between the original IASI and IASI-sonde corrected TCO_3. Thus, a limitation being that though the upper troposphere is the most sensitive region to ozone radiative properties, the scaling of the TO_3RE is applied based on the satellite-ozonesonde TCO_3 relative differences.

TOMCAT allows for a further quantification of the TO_3RE in the satellite-era and the ability to run sensitivity experiments to explore some important top-level processes. Evaluation of the model using the IASI products and ozonesondes (see **SI-2**, **Figure S3** & **S4**) shows the model generally captures the TCO_3 spatial pattern and absolute values. In the tropics (mid/high-latitudes), the model underestimates (overestimates) by approximately 10-20% on average. These biases are comparable with other modelling studies evaluating models against satellite TO_3 observations (e.g. Archibald et al., 2020; Monks et al., 2017; Nassar et al., 2009; Young et al., 2013), indicating TOMCAT to be suitable for this study.

The global mean TCO_3 from TOMCAT (2008-2017) (**Figure 2 – top panel**) is 30.7 DU and consistent with the IASI data sets in **Figure 1**. When translated into TO_3RE, described above, the peak values from TOMCAT range between 2.0 and >2.5 W/m^2 over Africa, Australia and the sub-tropics. The global area-weighted TO_3RE for TOMCAT is 1.26 W/m^2, thus slightly larger than for IASI (1.21-1.23 W/m^2). As TOMCAT has a positive TCO_3 bias with respect to the observations in the sub-tropics, where the TO_3RE influence is most pronounced, this probably explains the slightly larger model TO_3RE value. In the bottom panel of **Figure 2**, the zonal profiles (weighted by cosine of latitude to highlight the relative influence on the global weighted average) for TCO_3 (TO_3RE) have similar values to that of IASI. Here, the TOMCAT high-latitude values are near-zero (constrained by cos(90°) = 0), mid-latitude values range between 10.0 and 20.0 DU (0.5 to 1.0 W/m^2) and sub-tropical values range between 30.0 and 38.0 DU (1.5 and 1.7 W/m^2). There is a decrease to approximately 25.0 DU (1.0-1.3 W/m^2) in the tropics. In terms of the NTO_3RE, the TOMCAT global area-weighted average is 41.0 mW/m^2/DU, which is similar to IASI. The peak NTO_3RE values are over the oceans (50.0-60.0 mW/m^2/DU) and over Africa/Australia (>60.0 mW/m^2/DU).

3.2. Temporal Evolution of the Tropospheric Ozone Radiative Effect

Formatted: Outline numbered + Level: 2 + Numbering Style: 1, 2, 3, … + Start at: 1 + Alignment: Left + Aligned at: 0.63 cm + Indent at: 1.9 cm

As IASI has daily global coverage (Clerbaux et al., 2009), we are able to derive annual average 3D ozone fields between 2008 and 2017, thus providing the first assessment of interannual variability and decadal tendency in satellite derived TO_3RE. **Figure 3** shows the annual TO_3RE time series for all three IASI products. First thing to note is that the Eumetsat meteorological data used to retrieve ozone for the IASI-FORLI product is subject to discontinuities (Boynard et al., 2018; Wespes et al., 2018). As a result, we include decadal analysis of the IASI-FORLI data for the full time period (2008-2017) and then a sub-time period (2011-2017) given the large discontinuity in September 2010 reported by Boynard et al., (2018) and Wespes et al., (2018). Here, we can derive the TO_3RE to quantify the absolute values and how they compare between products over the two time periods. In the near future, a new consistent IASI-FORLI ozone climate data record will be available using a more stable set of level-2 Eumetsat meteorological data retrieved from MetOp IASI and microwave sounders.

For IASI-SOFRID and IASI-IMS, the annual TO_3RE values range between 1.19 and 1.24 W/m^2 across the 2008-2017 decade. IASI-FORLI has somewhat larger values at the start of the record (1.26-1.28 W/m^2) before tending to that of IASI-SOFRID/IASI-IMS from 2011 onwards. Correlations (squared) in the annual TO_3RE time-series between IASI-FORLI and IASI-SOFRID (IASI-IMS) are poor at R^2=0.148 (R^2=0.132). However, IASI-SOFRID and IASI-IMS have a much stronger agreement with R^2=0.591 sharing nearly 60% of the temporal variability. We also calculate the coefficient of variation (CoV, i.e., time series standard deviation divided by its mean) to assess the inter-annual variability. For IASI-SOFRID and IASI-IMS, this is 1.1%, but for IASI-FORLI it is 2.5%. Therefore, there is more year-to-year variability in the IASI-FORLI TO_3RE record. However, when focussing on IASI-FORLI data for 2011-2017, the CoV drops to 1.2% in-line with IASI-SOFRID and IASI-IMS. The correlation (squared) values are now $R^2_{FORLI-SOFRID}$=0.496 and $R^2_{FORLI-IMS}$=0.137, which shows improved agreement between IASI-FORLI and IASI-SOFRID, but slightly surprisingly not with IASI-IMS. This may potentially be due to the lower sampling sizes of the IASI-IMS data record. Using ordinary least squares fit regression, IASI-FORLI, IASI-SORFRID and IASI-IMS have global average weighted TO_3RE linear trends of -0.64 (-0.99, -0.28; 95% confidence interval) %/year, -0.01 (-0.14, 0.12) %/year and -0.13 (-0.36, 0.10) %/year (see **Table 1**). As the IASI-FORLI product has known discontinuities (hence the larger CoV), the near-zero IASI-SOFRID and IASI-IMS trends are more robust. This is supported by IASI-FORLI when only considering 2011-2017 with a linear trend of -0.21 (-0.66, 0.23) %/year. Therefore, this suggests negligible change in the contribution of TO_3 to the tropospheric radiative effect over the recent past (i.e. 2008-2017).

TOMCAT global average weighed TO_3RE ranges between 1.24 and 1.29 W/m^2 between 2008 and 2017. The CoV is 1.5% for TOMCAT and is comparable to the IASI products (i.e. IASI-FORLI for later years). The TOMCAT TO_3RE time-series also has similar temporal variability (e.g. peaks in 2008, 2010 and 2017 and troughs in 2009 and 2014 to that of the IASI products. The underlying TOMCAT TO_3RE decadal trend is -0.05 (-0.40, 0.30) %/year and consistent with the IASI products. So, between 2008 and 2017, there has been limited overall change in TO_3, despite reasonable interannual variability, and thus its decadal impact on the TO_3RE has been relatively minor.

To investigate the importance of emissions and meteorology on the decadal TO_3RE trends, TOMCAT was run twice for the full time-period, once using repeating emissions and once using repeating meteorology for 2008 (i.e. start of the time-series). Using fixed emissions reduced the TO_3 burden and the TO_3RE values dropped to 1.22 to 1.28 W/m^2 (i.e. minima in 2014 and 2015 more pronounced). However, the trend in TO_3RE (-0.23 (-0.59, 0.23) %/year) remained small indicating that temporal changes in emissions yield a relatively small influence on the decadal tendency in TO_3RE. By comparison with the fixed meteorology run, temporal changes in meteorological processes over the period 2008-17 were found not to dramatically alter the TO_3RE values either, but there is an increase to 1.26 to 1.30 W/m^2 when the model meteorology is fixed to 2008. The corresponding TO_3RE trend in the fixed meteorology run is 0.26 (0.13, 0.39) %/year leading to a steady increase in TO_3RE, though with a similar magnitude to that of the fixed emissions experiment. Therefore, temporal changes in pre-cursor emissions and meteorological processes appear to be balancing each other leading to the near-zero TOMCAT control run TO_3RE trend. However, the largest changes in TO_3RE between the control and fixed meteorology runs are towards the end of the decade, coinciding with the 2015/2016 El Niño event (i.e. TO_3 spatiotemporal variability has previously been linked to El Niño activity – e.g. Ziemke et al., (2015) and Rowlinson et al., (2019)). The largest difference between the TOMCAT control and fixed meteorology runs is 0.6 W/m^2 in 2015 Overall, the year-to-year variability in meteorology appears to be contracting any decadal TO_3RE trend arising from temporal changes in precursor emissions with the net result being no substantial underlying change in TO_3RE over the 2008-2017 decade.

Figure 4 shows the horizontal and vertical impact of the two sensitivity experiments on TOMCAT O_3 radiative effect (note the different colour bar scales). Consistent with **Figures 1** and **2**, the TOMCAT control TO_3RE has peak values (>2.50 W/m^2) over northern Africa and throughout the sub-tropics (approximately 2.0 W/m^2, **Figure 4a**). Vertically, the TOMCAT peak ozone radiative effect (>0.25 W/m^2) is in the upper troposphere (**Figure 4b**) with the largest impact in the sub-tropics of both hemispheres (500-200 hPa). Similar values extend through mid-latitudes of both hemispheres but in a smaller pressure range (400-300 hPa).

In **Figure 4c**, TO_3RE is seen to be higher in the fixed meteorology run than the control by 0.1 to >0.2 W/m^2 throughout the tropics and sub-tropics, although there is considerable spatial variability, including an area in the sub-tropical Pacific where TO_3RE is lower in the fixed meteorology run by -0.15 W/m^2. In high and mid-latitudes, TO_3RE is lower than the control by between -0.1 and 0.0 W/m^2. In the upper troposphere (**Figure 4d**), the zonal averaged contribution to TO_3RE in the fixed meteorology run is consistently higher than the control, by up to 0.02 W/m^2 at approximately 200 hPa in the tropics and sub-tropics and persisting at approximately 0.01 W/m^2 down to 600 hPa in the same latitudinal range. Poleward of 50°N and 50°S, TO_3RE is lower in the fixed meteorology run, peaking at -0.02 to -0.015 W/m^2 at 300 hPa and extending down to 500 hPa at -0.005 W/m^2.

With fixed emissions, TO_3RE is higher at northern mid- and high latitudes by up to 0.02 W/m^2, whereas in the tropics/sub-tropics and southern mid-latitudes it is generally lower than in the control run by up to -0.02 W/m^2 (**Figure 4e**). However, over tropical Asia, Indonesia and Australia, TO_3RE is seen to be lower by a more substantial amount, -0.05 to -0.04 W/m^2. In regard to its height dependence, contributions to TO_3RE are seen in **Figure 4f** to be lower in the fixed emissions run by up to -0.005 W/m^2 in the tropics/sub-tropics between 600 and 200 hPa, and also in a tongue stretching to southern high latitudes at around 300hPa (**Figure 4f**). In the northern hemisphere, on the other hand, TO_3RE in the layer between 400 and 600 hPa is seen to be higher by up to 0.003 at latitudes from the pole to 50°N, and down to higher pressures at latitudes below 50°N.

In summary, the two model sensitivity experiments indicate that, except for southern high latitudes, precursor emissions and meteorology exerted counteracting influences of comparable magnitude on TO_3RE in the 2008-17 decade, and this is specifically so in the sub-tropical regions of the upper troposphere, where contributions to global average area weighted TO_3RE are largest. At southern high latitudes, precursor emissions and meteorology are seen to have both increased TO_3RE over this period, specifically through contributions in the uppermost troposphere, although area weighting minimized their combined impact in the global averaged TO_3RE.

~~**1. Results**~~

~~**1.1. Tropospheric Ozone Radiative Effect**~~

Formatted: Indent: Left: 0.63 cm, Hanging: 0.63 cm, Outline numbered + Level: 1 + Numbering Style: 1, 2, 3, … + Start at: 1 + Alignment: Left + Aligned at: 0.63 cm + Indent at: 1.27 cm

Formatted: Indent: Left: 0.63 cm, Outline numbered + Level: 2 + Numbering Style: 1, 2, 3, … + Start at: 1 + Alignment: Left + Aligned at: 0.63 cm + Indent at: 1.9 cm

Figure 1 shows the IASI derived TCO_3, TO_3RE and normalised TO_3RE (NTO_3RE, i.e. the TO_3RE divided by its TCO_3 as in Rap et al., (2015)). For the TCO_3, all three harmonised IASI products have good spatial agreement in the long-term (2008-2017) average with a background north-south hemisphere gradient of approximately 30.0-40.0 to 15.0-25.0 DU. Peak TCO_3 (>40.0 DU) occurs over East Asia, the Middle East and ozone outflow from central Africa (e.g. from lightning and biomass burning precursor gases (Moxim & Levy, 2000)). The global average TCO_3 values for IASI-FORLI, IASI-SOFRID and IASI-IMS are 32.6 DU, 29.9 DU and 29.9 DU, respectively (**Figure 1 left column**).

When the TO_3RE is calculated (**Figure 1 middle column**), peak values occur over the sub-tropics, Africa and Australia ranging between approximately 2.0 and 2.5 W/m^2 consistently for each IASI product. The minimum values are in the high latitudes ranging between 0.0 and 0.8 W/m^2 where TO_3 appears to have limited impact on the TO_3RE. The bottom panel of **Figure 1** supports this as the zonally average profiles, weighted by the cosine of degrees latitude, show that TCO_3 is near-zero in the high-latitudes, approximately 15.0-20.0 DU in the mid-latitudes, peaking at 28.0-33.0 DU in the sub-tropics and then decreasing by several DU at the tropics. The corresponding TO_3RE profiles follow a similar pattern with near-zero values at the high-latitudes, approximately 0.5-1.0 W/m^2 in the mid-latitudes, peak at 1.5 W/m^2 in the sub-tropics and then decrease to 1.1-1.2 W/m^2 in the tropics. Therefore, the sub-tropics have the largest contribution to the global TO_3RE. The global weighted TO_3RE averages for IASI-FORLI, IASI-SOFRID and IASI-IMS are 1.23, 1.21 and 1.21 W/m^2, respectively.

The NTO_3RE (**Figure 1 right column**) provides an estimate of where the TO_3RE is most sensitive to changes in TCO_3 (i.e. the unit of TO_3RE per unit of TCO_3). Peak NTO_3RE (>45.0 $mW/m^2/DU$) occurs in similar locations to the peak TO_3RE (e.g. sub-tropics, Africa and Australia), while the minimum values (10.0-20.0 $mW/m^2/DU$) occur in the high-latitudes. However, while the South Pacific TCO_3 values (23.0-30.0) are lower than other ocean regions (e.g. >30.0 DU), the NTO_3RE values are of similar magnitude (approximately 50.0 $mW/m^2/DU$). Therefore, while the sub-tropical/mid-latitude oceans have reasonable large TCO_3 and TO_3RE values, the South Pacific is more effective at contributing to the TO_3RE, despite its lower TCO_3 values (i.e. more positive radiative effect per unit of TO_3).

Overall, the global weighted average NTO_3RE is 37.78, 40.43 and 40.60 $mW/m^2/DU$ for IASI-FORLI, IASI-SORID and IASI-IMS, respectively. Based on the AKs, the tropospheric degrees of freedom of signal (DOFS, between the surface and 170 hPa – approximate tropopause) is approximately 1.0 for all three IASI products (not shown here). However, it is likely that differences in the IASI ozone profiles are driving the contrasting globally averaged NTO_3RE values. As the IASI-FORLI NTO_3RE is lower, while having the highest global average TCO_3 and TO_3RE, it suggests that IASI-FORLI has more TO_3 in the mid-troposphere where the radiative kernel has less sensitivity. Further to this, as the IASI ozone products only have approximately 1.0 DOFS, the harmonisation of the products using the ozonesondes can only be done on a tropospheric column level and thus the scaling of the satellite derived TO_3RE (i.e. even though the upper troposphere is the most sensitive region to ozone radiative properties, the scaling of the TO_3RE is applied based on the satellite-ozonesonde TCO_3 relative differences).

TOMCAT allows for a further quantification of the TO_3RE in the satellite-era and the ability to run sensitivity experiments to explore important processes. Therefore, the TOMCAT equivalent metrics from **Figure 1** are presented in **Figure 2**. Evaluation of the model using the IASI products and ozonesondes (see **SI 2**, **Figure S3** & **S4**) shows the model generally captures the TCO_3 spatial pattern and absolute values. In the tropics (mid/high-latitudes), the model underestimates (overestimates) by approximately 10-20% on average. These biases are comparable with other modelling studies evaluating models against satellite TO_3 observations (e.g. Archibald et al., 2020; Monks et al., 2017; Nassar et al., 2009; Young et al., 2013), indicating that TOMCAT is a suitable modelling framework in this study.

The globally mean TCO_3 from TOMCAT (2008-2017) with the three sets of AKs applied (**Figure 2 left column**) ranges between 31.6 and 32.5 DU, so it slightly larger than the IASI data sets in **Figure 1**. When translated into TO_3RE, the peak values from TOMCAT (with AKs applied) ranges between 2.0 and >2.5 W/m^2 over Africa, Australia and the sub-tropics. The globally weighted TO_3RE for TOMCAT with the IASI-FORLI and IASI-SOFRID AKs applied is 1.28 W/m^2 and thus moderately higher than IASI (1.21-1.23 W/m^2) but comparable overall. However, the globally weighted TO_3RE for TOMCAT with IASI-IMS AKs applied is larger at 1.34 W/m^2. As TOMCAT has a positive TCO_3 bias with the observations in the sub-tropics, where the TO_3RE influence is most pronounced, this probably explains the larger model TO_3RE values. In the bottom panel of **Figure 2**, the zonal profiles (weighted by cosine of degree latitude) for TCO_3 (TO_3RE) are consistent with IASI as high-latitude values are near-zero, mid-latitude values range between 10.0 and 20.0 DU (0.5 to 1.0 W/m^2) and sub-tropical values range between 30.0 and 38.0 DU (1.5 and 1.7 W/m^2). There is a decrease to approximately 25.0 DU (1.0-1.3 W/m^2) in the tropics. In terms of the NTO_3RE, the TOMCAT (with AKs applied) global weighted values range between 39.4 and 42.4 mW/m^2/DU, which is similar to IASI. The peak NTO_3RE values are over the oceans (50.0-60.0 mW/m^2/DU) and over Africa/Australia (>60.0 mW/m^2/DU). Like for IASI, the TCO_3 values over the South Pacific are lower than the other ocean values but the NTO_3RE values are similar, again showing that despite the lower TO_3, the South Pacific region is important for the global TO_3RE given its greater sensitivity (i.e. more radiative effect per unit of TO_3).

1.2. Temporal Evolution of the Tropospheric Ozone Radiative Effect

As IASI has daily global coverage (Clerbaux et al., 2009), we are able to derive annual average 3D ozone fields between 2008 and 2017, thus providing the first assessment of temporal variability and tendency in satellite-derived TO_3RE. **Figure 3** shows the annual TO_3RE time series for all three IASI products. First thing to note, is that the Eumetsat meteorological data used to retrieve ozone for the IASI-FORLI product is subject to inhomogeneities (Boynard et al., 2018; Wespes et al., 2018). As a result, we include long-term analysis of the IASI-FORLI data for the full time period (2008-2017) and then a sub-time period (2011-2017) given the large inhomogeneity in September 2010 reported by Boynard et al., (2018) and Wespes et al., (2018). Here, we can derive the TO_3RE to quantify the absolute values (e.g. are they generally similar year to year) and how they compare between products over the two time periods. In the near future, a new consistent IASI-FORLI ozone climate data record will be available using homogeneous level-2 Eumetsat meteorological data.

For IASI-SOFRID and IASI-IMS, the annual TO_3RE values range between 1.19 and 1.24 W/m^2 across the 2008-2017 time period. IASI-FORLI has somewhat larger values at the start of the record (1.26-1.28 W/m^2) before tending to that of IASI-SOFRID/IASI-IMS from 2011 onwards. Correlations (squared) in the annual TO_3RE time-series between IASI-FORLI and IASI-SOFRID (IASI-IMS) are poor at R^2=0.148 (R^2=0.132). However, IASI-SOFRID and IASI-IMS have a much stronger agreement with R^2=0.591 (significant at the 95th confidence level, CL95%) sharing nearly 60% of the temporal variability. We also calculate the coefficient of variation (CoV, i.e., time series standard deviation divided by its mean) to assess the inter-annual variability. For IASI-SOFRID and IASI-IMS, this is 1.1%,

Formatted: Indent: Left: 0.63 cm, Outline numbered + Level: 2 + Numbering Style: 1, 2, 3, … + Start at: 1 + Alignment: Left + Aligned at: 0.63 cm + Indent at: 1.9 cm

but for IASI-FORLI it is 2.5%. Therefore, there is more year-to-year variability in the IASI-FORLI TO_3RE record. However, when focussing on IASI-FORLI data for 2011-2017, the CoV drops to 1.2% in-line with IASI-SOFRID and IASI-IMS. The correlation (squared) values are now $R^2_{FORLI-SOFRID}$=0.496 (significant at the CL95%) and $R^2_{FORLI-IMS}$=0.137, which shows improved agreement between IASI-FORLI and IASI-SOFRID, but slightly surprisingly not with IASI-IMS. Using ordinary least squares fit regression, IASI-FORLI, IASI-SORFRID and IASI-IMS have global average weighed TO_3RE linear trends of -0.6%/year (CL95%), 0.0%/year (non-significant) and -0.1%/year (non-significant). As the IASI-FORLI product has known inhomogeneities (hence the larger CoV), the insignificant IASI-SOFRID and IASI-IMS trends are more robust. This is supported by IASI-FORLI when only considering 2011-2017 with an insignificant linear trend of -0.2%/year. Therefore, this suggests negligible change in the contribution of TO_3 to the tropospheric radiative effect and thus climate over the recent past (i.e. 2008-2017).

TOMCAT global average weighed TO_3RE (without AKs applied) ranges between 1.24 and 1.29 W/m^2 between 2008 and 2017. The CoV is 1.5% for TOMCAT, so it is larger than both IASI-SOFRID and IASI-IMS. When the IASI AKs are applied to TOMCAT, there is a substantial shift in the modelled absolute TO_3RE values. TOMCAT with IASI-SOFRID and IASI-FORLI AKs applied ranged between 1.28 and 1.30 W/m^2. And for TOMCAT with the IASI-IMS AKs applied, the TO_3RE values peak at 1.33 to 1.34 W/m^2 between 2008 and 2017. As well as the increase in TO_3RE values, the application of the AKs squashes the TOMCAT inter-annual variability with corresponding CoV values between 0.4 and 0.6%, which is smaller than the original CoV of 1.5%. Interestingly, without the application of the AKs, the TOMCAT TO_3RE time-series has similar temporal variability (e.g. peaks in 2008, 2010 and 2017 and troughs in 2009 and 2014. Overall, all the TOMCAT TO_3RE time-series (with and without AKs applied have insignificant linear trends ranging between -0.1%/year and 0.1%/year. Therefore, even with the influence of the IASI AKs on the TOMCAT TO_3RE time-series, there appears to be a negligible trend in the modelled TO_3RE, supporting that of the IASI records. As a result, between 2008 and 2017, there has been limited change in TO_3 and TO_3RE, thus the impact of TO_3 on climate has remained stable.

To investigate the importance of emissions and meteorology on the long-term TO_3RE trends, TOMCAT was run using repeating emissions and repeating meteorology for 2008 (i.e. start of the time-series) in two sensitivity experiments for the full time-period. Here, we find that in absolute terms, using fixed emissions reduces the TO_3 burden and the TO_3RE as the time-series drops to 1.22 to 1.28 W/m^2 (i.e. minima in 2014 and 2015 more pronounced). However, the trend in TO_3RE (-0.2%/year) remains insignificant and that emissions are only moderately important in driving long-term tendencies in TO_3RE. On the other hand, meteorological factors, while not dramatically altering the absolute simulated TO_3RE values, are more important as fixing the meteorology yields a steady and significant increase (0.3%/year). Thus, without year-to-year variability in meteorology, temporal variability in TO_3 would likely have a more substantial impact on the present day climate.

Figure 4 shows the horizontal and vertical impact of the two sensitivity experiments on TOMCAT O_3 radiative effect (note the different colour bar scales). Consistent with **Figures 1** and **2**, the TOMCAT control TO_3RE has peak values (>2.50 W/m^2) over northern Africa and throughout the sub-tropics (approximately 2.0 W/m^2, **Figure 4a**). Vertically, the TOMCAT peak ozone radiative effect (>0.25 W/m^2) is in the upper troposphere (**Figure 4b**) with the largest impact in the sub-tropics of both hemispheres (500-200 hPa). Similar values extend through the hemispheric mid-latitudes but in a smaller pressure range (400-300 hPa). As shown in **Figure 3**, the fixed meteorological run imposes a significant TO_3RE trend on the modelled tendency between 2008 and 2017. From **Figure 4c**, the

~~difference between the fixed meteorology and control runs shows mainly positive TO$_3$RE differences of 0.1 to >0.2 W/m^2 throughout the tropics and sub-tropics, though there is considerable spatial variation due to changes in the global circulation. In the high and mid-latitudes, there are smaller scale negative differences ranging between -0.1 and 0.0 W/m^2 (though some differences up to -0.15 W/m^2 in the sub-tropical Pacific). In the upper troposphere (**Figure 4d**), the zonal average O$_3$ radiative effect is consistent with positive differences of up to 0.02 W/m^2 at approximately 200 hPa in the tropics and sub-tropics. The positive differences (approximately 0.01 W/m^2) filter down to 600 hPa in the same latitudinal range. In the mid-latitudes, the peak negative differences are approximately -0.02 to -0.015 W/m^2 at 300 hPa, with a reach down to 500 hPa at -0.005 W/m^2. Overall, as shown in **Figure 3**, the fixed meteorology run increases the global average TO$_3$RE. While this could be a specific signal related to the 2008 meteorology (i.e. it is conducive to TO$_3$ formation), it clearly shows that the upper tropospheric tropical and sub-tropical regions predominantly control the global TO$_3$RE average and its temporal variability (i.e. the region where the meteorological inter-annual variability is buffering underlying increases in TO$_3$RE). With fixed emissions, there is a general increase (decrease) in TO$_3$RE in the tropics/sub-tropics (northern mid-latitudes) by 0.02 (-0.02) W/m^2. However, over tropical Asia, Indonesia and Australia, the decrease in TO$_3$RE is more substantial at -0.05 to -0.04 W/m^2 (**Figure 4e**). Vertically, there are decreases (increases) in the O$_3$ radiative effect of -0.005 (0.003) W/m^2 in the tropics/sub-tropics (northern mid-latitudes) between 600 and 200 (800 and 400) hPa (**Figure 4f**). Overall, the meteorological variability, in comparison to the long-term emission changes in O$_3$ precursor gases, has substantially more influence on the inter-annual variability of the global TO$_3$RE over this decade.~~

~~2.~~4. Conclusions

By using state-of-the-art satellite ozone profile retrievals from the Infrared Atmospheric Sounding Interferometer (IASI), on-board MetOp-A, in combination with the TOMCAT chemical transport model (CTM) and the offline radiative transfer model, SOCRATES, we provide an updated estimate of the tropospheric ozone radiative effect (TO$_3$RE) and provide the first observational constraint on its variability over the decade 2008-2017. Building upon the previous study of Rap et al., (2015), who quantified the globally weighed average TO$_3$RE to be 1.17±0.03 W/m^2 (based on data between 2005 and 2008), we find the ~~long-term~~ decadal average TO$_3$RE, between 2008 and 2017, to range from 1.21 and 1.26~~8~~ W/m^2. This represents an update on the estimates from Rap et al., 2015) using an improved version of the TOMCAT model (as in Monks et al., (2017) compared to Richards et al., 2013)) and improved satellite products with better spatial and temporal coverage. However, these two studies do cover different time periods, which may be contributing to the differences between the studies. Secondly, neither the modelled, nor the observed TO$_3$RE suggest any substantial change during this ~~period~~decade. ~~Therefore, the tropospheric ozone contribution to climate, through its infrared radiative properties, has remained stable with time during 2008-2017.~~ Investigations of the importance of ozone precursor emissions and meteorology, through targeted sensitivity experiments repeating emissions and meteorology for 2008 (i.e. year at start of time-series), suggest that temporal changes in both factors have counteracted each other. Fixing emissions reduces the TO$_3$RE values/tendency, so changes in emissions are driving a steady increase in TO$_3$RE. Conversely, fixing the meteorology drives an increase the TO$_3$RE values/tendency, thus is yielding to a net decrease in TO$_3$RE despite its large variability. Therefore, the net tropospheric ozone contribution to atmospheric radiative properties, and potentially climate, has remained relatively stable with time during 2008-2017.

Formatted: Indent: Left: 0.63 cm, Hanging: 0.63 cm, Outline numbered + Level: 1 + Numbering Style: 1, 2, 3, … + Start at: 1 + Alignment: Left + Aligned at: 0.63 cm + Indent at: 1.27 cm

Formatted: Not Highlight

Formatted: Not Highlight

~~emissions have a limited impact on the globally weighted average TO_3RE. Meanwhile, fixing the meteorology to a specific year (i.e. 2008) introduces a significant positive trend in global TO_3RE, indicating that the meteorological variability in the tropical/sub-tropical upper troposphere has been important in stabilising the tropospheric ozone contribution to climate, via radiative properties, in the recent past (i.e. satellite-era).~~

Acknowledgements

This work was funded by the UK Natural Environment Research Council (NERC) by providing funding for the National Centre for Earth Observation (NCEO, award reference NE/R016518/1) and funding from the European Space Agency (ESA) Climate Change Initiative (CCI) post-doctoral fellowship scheme (award reference 4000137140). The TOMCAT runs were undertaken on ARC3, part of the High-Performance Computing facilities at the University of Leeds, UK. The IASI-SOFRID research was conducted at LAERO with some financial support from the CNES French spatial agency (TOSCA–IASI project). We thank the AC SAF project of the EUMETSAT for providing data and/or products used in this paper. Anna Maria Trofaier (ESA Climate Office) provided support and advice throughout the fellowship.

Formatted: Font: (Default) +Body (Calibri), 12 pt

Formatted: Font: 12 pt

Formatted: Font: 12 pt

Formatted: Font: 12 pt

Formatted: Font: (Default) +Body (Calibri), 11 pt

Data Availability

The IASI-FORLI and IASI-SOFRID data can be obtained from https://iasi.aeris-data.fr/O3 and https://iasi-sofrid.sedoo.fr/. The IASI-IMS data is available via the NERC Centre for Environmental Data Analysis (CEDA) Jasmin platform subject to data requests. However, the IASI-IMS data and TOMCAT simulations used in this study are available from https://homepages.see.leeds.ac.uk/~earrjpo/to3re/. The ozonesonde data for WOUDC, SHADOZ and NOAA is available from https://woudc.org/, https://tropo.gsfc.nasa.gov/shadoz/ and https://gml.noaa.gov/ozwv/ozsondes/.

Author Contributions

RJP conceptualised, planned and undertook the research study. AR provided the SOCRATES radiative kernel. BB, ELF, BJK, RS, BGL, LJV, AB and CW provided the IASI ozone data and advice on using the products. MAP performed the TOMCAT model simulations with support from MPC and WF. CR provided advice and help during RP's ESA CCI fellowship. RJP prepared the manuscript with contributions from all co-authors.

Conflicts of Interest

The authors declare no conflicts of interest.

References

Archibald, A.T., O'Connor, F.M., Abraham, N.A., et al. 2020. Description and evaluation of the UKCA stratosphere–troposphere chemistry scheme (StratTrop vn 1.0) implemented in UKESM1. *Geoscientific Model Development*, **13**, 1223–1266, doi: 10.5194/gmd-13-1223-2020.

Barret, B., Le Flochmoen, E., Sauvage, B., et al. 2011. The detection of post-monsoon tropospheric ozone variability over south Asia using IASI data. *Atmospheric Chemistry and Physics*, **11**, 9533-9548, doi: 10.5194/acp-11-9533-2011.

Barret, B., Emili, E., Le Flochmoen, E. 2020. A tropopause-related climatological a priori profile for IASI-SOFRID ozone retrievals: improvements and validation. *Atmospheric Measurement Techniques*, **13**, 5237–5257, doi: 10.5194/amt-13-5237-2020.

~~Bethan, S., Vaughan, G. and Reid, S.J. 1996. A comparison of ozone and thermal tropopause heights and the impact of tropopause definition on quantifying the ozone content of the troposphere. *Journal of Quantitative Spectroscopy and Radiative Transfer*, 122: 929-944, doi: 10.1002/qj.49712253207.~~

Bowman, K.W., Shindell, D.T., Worden, H.M., et al. 2013. Evaluation of ACCMIP outgoing longwave radiation from tropospheric ozone using TES satellite observations. *Atmospheric Chemistry and Physics*, 13, 4057-4072, doi: 10.5194/acp-13-4057-2013.

Boynard, A., Hurtmans, D., Garane, K., et al. 2018. Validation of the IASI FORLI/EUMETSAT ozone products using satellite (GOME-2), ground-based (Brewer-Dobson, SAOZ, FTIR) and ozonesonde measurements. *Atmospheric Measurement Techniques*, **11 (9)**, doi: 10.5194/amt-11-5125-2018.

Chipperfield, M.P. 2006. New version of the TOMCAT/SLIMCAT off-line chemistry transport model: Intercomparison of stratospheric trace experiments. *Quarterly Journal of the Royal Meteorological Society*, **132**, 1179–1203, doi:10.1256/qj.05.5.

Clerbaux, A., Boynard, A., Clarisse, L., et al. 2009. Monitoring of atmospheric composition using the thermal infrared IASI/MetOp sounder. *Atmospheric Chemistry and Physics*, **9**, 6041–6054, doi: 10.5194/acp-9-6041-2009.

Dee, D.P., Uppala, S.M., Simmons, A.J., et al.: The ERA-Interim reanalysis: Configuration and performance of the data assimilation system*, Quarterly Journal of the Royal Meteorological Society*, 137 (656), 553–597, doi:10.1002/qj.828, 2011.

Dlugokencky, E. 2020. NOAA Global Monitoring Laboratory–Trends in Atmospheric Methane, Available at: https://gml.noaa.gov/ccgg/trends_ch4/ (last accessed 23/01/2023).

Doniki, S., Hurtmans, D., Clarisse, et al. 2015. Instantaneous longwave radiative impact of ozone: an application on IASI/MetOp observations, *Atmospheric Chemistry and Physics*, **15**, 12971–12987, doi:10.5194/acp-15-12971-2015.

Edwards, J.M and Slingo, A. 1996. Studies with a flexible new radiation code. I: Choosing a configuration for a large-scale model. *Quarterly Journal of the Royal Meteorological Society*, **122**, 689–719, doi:10.1002/qj.49712253107.

Fels, S.B., Mahlman, J.D., Schwarzkopf, M.D., et al. 1980. Stratospheric Sensitivity to Perturbations in Ozone and Carbon Dioxide: Radiative and Dynamical Response. *Journal of Atmospheric Science*, **37**, 2265-2297, doi: 10.1175/1520-0469(1980)037<2265:Sstpio>2.0.Co;2.

Feng, L., Smith, S. J., Braun, C., et al. 2020. The generation of gridded emissions data for CMIP6. *Geoscientific Model Development*, **13**, 461–482, doi:10.5194/gmd-13-461-2020.

Fleming ZL, Doherty RM, von Schneidemesser E, Malley CS, Cooper OR, Pinto JP, Colette A, Xutt X, Simpson D, Schultz MG, Lefohn AS, Hamad S, Moolla R, Solberg S and Feng Z.: Tropospheric Ozone Assessment Report: Present-day ozone distribution and trends relevant to human health. *Elem Sci Anth*, **6**(12), doi: 10.1525/elementa.273, 2018.

Forster, P., Storelvmo, T., Armour, K., Collins, W., Dufresne, J.- L., Frame, D., Lunt, D. J., Mauritsen, T., Palmer, M. D., Watanabe, M., Wild, M., and Zhang, H.: The Earth's Energy Budget, Climate Feedbacks, and Climate Sensitivity, in: Climate Change 2021: The Physical Science Basis, Contribution of Working Group I to the Sixth Assessment Report of the Intergovernmental Panel on Climate Change, edited by: Masson-Delmotte, V., Zhai, P., Pirani, A., Connors, S. L., Péan, C., Berger, S., Caud, N., Chen, Y., Goldfarb, L., Gomis, M. I., Huang, M., Leitzell, K., Lonnoy, E., Matthews, J. B. R.,Maycock, T. K., Waterfield, T., Yelekçi, O., Yu, R., and Zhou, B., Cambridge University Press, Cambridge, United Kingdom and New York, NY, USA, 923– 1054, doi:10.1017/9781009157896.009, 2021.

Gauss, M., Myhre, G., Isaksen, S.A., et al. 2006. Radiative forcing since preindustrial times due to ozone change in the troposphere and the lower stratosphere. *Atmospheric Chemistry and Physics*, **6**, 575-599, doi: 10.5194/acp-6-575-2006.

Gulev, S.K., P.W. Thorne, J. Ahn, F.J. Dentener, C.M. Domingues, S. Gerland, D. Gong, D.S. Kaufman, H.C. Nnamchi, J. Quaas, J.A. Rivera, S. Sathyendranath, S.L. Smith, B. Trewin, K. von Schuckmann, and R.S. Vose.: Changing State of the Climate System. In Climate Change 2021: The Physical Science Basis. Contribution of Working Group I to the Sixth Assessment Report of the Intergovernmental Panel on Climate Change, edited by Masson-Delmotte, V., P. Zhai, A. Pirani, S.L. Connors, C. Péan, S. Berger, N. Caud, Y. Chen, L. Goldfarb, M.I. Gomis, M. Huang, K. Leitzell, E. Lonnoy, J.B.R. Matthews, T.K. Maycock, T. Waterfield, O. Yelekçi, R. Yu, and B. Zhou., Cambridge University Press, Cambridge, United Kingdom and New York, NY, USA, pp. 287–422, doi:10.1017/9781009157896.004, 2021.

Heue, K.P., Cold-Egbers, M., Delcloo, A., et al. 2016. Trends of tropical tropospheric ozone from 20 years of European satellite measurements and perspectives for the Sentinel-5 Precursor. *Atmospheric Measurement Techniques*, **9**, 5037-5051, doi: 10.5194/amt-9-5037-2016.

Hurtmans, D., Coheur, P.-F., Wespes, C., et al. 2012. FORLI radiative transfer and retrieval code for IASI, *Journal of Quantitative Spectroscopy and Radiative Transfer*, **113**, 1391–1408, doi:10.1016/j.jqsrt.2012.02.036. Iglesias-Suarez, F., Kinnison, D.E., Rap, A., et al. 2018. Key drivers of ozone change and its radiative forcing over the 21st century. *Atmospheric Chemistry and Physics*, **18**, 6121-6139, doi:10.5194/acp-18-6121-2018.

IASI-IMS. 2022. IASI-IMS Data [Dataset], https://homepages.see.leeds.ac.uk/~earrjpo/to3re/iasi_ims/ (last accessed 01/01/2023).

IASI-FORLI. 2020. Daily IASI/Metop-A ULB-LATMOS ozone (O3) L2 product (total column and vertical profile) (v20151001) [Dataset], https://iasi.aeris-data.fr/catalog/ (last accessed 15/12/2022).

IASI-SOFRID. 2022. Welcome to the IASI-SOFRID database (vn3.5) [Dataset], http://thredds.sedoo.fr/iasi-sofrid-o3-co/ (last accessed 01/12/2022).

Iglesias-Suarez, F., Kinnison, D.E., Rap, A., et al. 2018. Key drivers of ozone change and its radiative forcing over the 21st century. *Atmospheric Chemistry and Physics*, **18**(9), 6121-6139, doi: 10.5194/acp-18-6121-2018.

Joiner, J., Schoeberl, R.M., Vasilkov, A.P., et al. 2009. Accurate satellite-derived estimates of the tropospheric ozone impact on the global radiation budget. *Atmospheric Chemistry and Physics*, **9**, 4447-4465, doi: 10.5194/acp-9-4447-2009.

Keppins, A., Lambert, J.C., Granville, J., et al. 2018. Quality assessment of the Ozone_cci Climate Research Data Package (release 2017) – Part 2: Ground-based validation of nadir ozone profile data products. *Atmospheric Measurement Techniques*, **11**, 3769-3800, doi: 10.5194/amt-11-3769-2018.

Lamarque, J.F., Bond, T.C., Eyring, V., et al. 2010. Historical (1850-2000) gridded anthropogenic and biomass burning emissions of reactive gases and aerosols: methodology and application. *Atmospheric Chemistry and Physics*, **10**, 7017-7039, doi: 10.5194/acp-10-7017-2010.

Mann, G.W., Carslaw, K.S., Spracklen, D.V., et al. 2010. Description and evaluation of GLOMAP-mode: A modal global aerosol microphysics model for the UKCA composition-climate model. *Geoscientific Model Development*, **3**(2), 519– 551, doi:10.5194/gmd-3-519-2010.

McPeters, R.D., Labow, G.J., and Logan, J.A. 2007. Ozone climatological profiles for satellite retrieval algorithms. *Journal of Geophysical Research*, **112** (D05308), https://doi.org/10.1029/2005JD006823.

Mills G, Pleijelt H, Malley CS, Sinha B., Cooper OR, Schultz MG, Neufeld HS, Simpson D, Sharps K, Feng Z, Gerosa G, Harmens H, Kobayashi K, Saxena P, Paoletti E, Sinha V and Xu X.: Tropospheric Ozone Assessment Report: Present-day tropospheric ozone distribution and trends relevant to vegetation. *Elem Sci Anth*, 6(47), doi: 10.1525/elementa.302, 2018.

Monks, S.A., Arnold, S.R., Hollaway, M.J., et al. 2017. The TOMCAT global chemistry transport model v1.6: Description of chemical mechanism and model evaluation. *Geoscientific Model Development*, **10**(8), 3025– 3057, doi:0.5194/gmd-10-3025-2017.

Morgenstern, O., Hegglin, M.I., Rozanov, E., et al. 2017. Review of the global models used with phase 1 of the Chemistry-Climate Model Initiative (CCMI). *Geoscientific Model Development*, **10**(2), 639– 671, doi:10.5194/gmd-10-639-2017.

Moxy, W.J. and Levy, H. 2000. A model analysis of tropical South Atlantic Ocean tropospheric ozone maximum: The interaction of transport and chemistry. *Journal of Geophysical Research*, **105** (D13), 17393-17415, doi:10.1029/2000JD900175.

Myhre, G., Shindell, D., Breon, F.M., et al. 2013. Anthropogenic and Natural Radiative Forcing, in: Climate Change 2013: The Physical Science Basis. Contribution of Working Group I to the Fifth Assessment Report of the Intergovernmental Panel on Climate Change Cambridge University Press, Cambridge, United Kingdom and New York, NY, USA, 659–740.

Nassar, R., Logan, J.A., Mergretskaia, I.A., et al. 2009. Analysis of tropical tropospheric ozone, carbon monoxide, and water vapor during the 2006 El Niño using TES observations and the GEOS-Chem model. *Journal of Geophysical Research: Atmospheres*, **114 (D17304)**, doi: 10.1029/2009JD011760.

NOAA. 2023. ESRL/GML Ozonesondes [Dataset], https://gml.noaa.gov/ozwv/ozsondes/ (last accessed 01/06/2022).

Olivier, J., Peters, J., Granier, C., et al. 2003. Present and future surface emissions for atmsopheric compounds, *POET report #2*, Available at: http://accent.aero.jussieu.fr/Documents/del2_final.doc (last accessed 23/01/2023).

Pacifico, F., Harrison, S.P., Jones, C.D., et al. 2011. Evaluation of a photosynthesis-based biogenic isoprene emission scheme in JULES and simulation of isoprene emissions under present-day climate conditions, *Atmospheric Chemistry and Physics,* **11**, 4371–4389, doi**:**10.5194/acp-11-4371-2011.

Pimlott, M.A., Pope, R.P., Kerridge, B.J., et al. 2022. Investigating the global OH radical distribution using steady-state approximations and satellite data. *Atmospheric Chemistry and Physics,* **22**, 10467-10488, doi: 10.5194/acp-22-10467-2022.

Pope, R.J., Kerridge, B.J., Siddans, R., Latter, B.G., Chipperfield, M.P., Arnold, S.R., Ventress, L.J., Pimlott, M.A., Graham, A.M., Knappett, D.S and Rigby R.: Large Enhancements in Southern Hemisphere Satellite-Observed Trace Gases Due to the 2019/2020 Australian Wildfires. *Journal of Geophysical Research: Atmospheres,* **126**(18), e2021JD034892, doi: 10.1029/2021JD034892, 2021.

Rap, A., Richard, N.A.D., Forster, P.M., et al. 2015. Satellite constraint on the tropospheric ozone radiative effect. *Geophysical Research Letters*, **42**, 5074–5081, doi: 10.1002/2015GL064037.

Richards, N.A.D, Osterman, G.B., Browell, E.V., et al. 2008. Validation of tropospheric emission spectrometer ozone profiles with aircraft observations during the intercontinental chemical transport experiment–B. *Journal Geophysical Research*, **113**(D16S29), doi: 10.1029/2007JD008815.

Rodgers, C.D. 2000. Inverse methods for atmospheric sounding: Theory and practice. New Jersey, USA: World Science.

Rossow, W.B. and Schiffer, R.A.: Advances in understanding clouds from ISCCP, *Bulletin of the American Meteorological Society*, **80**(11), 2261–2287, doi:10.1175/1520-0477(1999)080<2261:aiucfi>2.0.co;2,1999.

Rowlinson, M.J., Rap, A., Arnold, S.R., Pope, R.J., Chipperfield, M.P., McNorton, J., Forster, P., Gordon, H., Pringle, K.J., Feng, W., Kerridge, B.J., Latter, B.G., Siddans, R.: Impact of El Nino-Southern Oscillation on the interannual variability of methane and tropospheric ozone. Atmospheric Chemistry and Physics, **19** (13), 8669-8686, doi: 10.5194/acp-19-8669-2019, 2019.

Rowlinson, M.J., Rap, A., Hamilton, D.S., et al. 2020. Tropospheric ozone radiative forcing uncertainty due to pre-industrial fire and biogenic emissions. *Atmospheric Chemistry and Physics*, **20**, 10937-10951, doi: 10.5194/acp-20-10937-2020.

Saunders, R., Matricardi, M., and Brunel, P. 1999. An improved fast radiative transfer model for assimilation of satellite radiance observations. *Quarterly Journal of the Royal Meteorological Society*, **125** (556 part B), 1407–1425, doi:10.1256/smsqj.55614.

Scott, C.E., Monks, S.A., Spracklen, D.V., et al. 2018. Impact on short-lived climate forcers increases projected warming due to deforestation. *Nature Communications*, **9**, 157, doi: 10.1038/s41467-017-02412-4.

Sellar, A.A., Jones, C.G., Mulcahy, J.P., et al. 2019. Description and Evaluation of the UK Earth System Model. *Journal of Advances in Modeling Earth Systems*, **11**, 4513-4558, doi: 10.1029/2019MS001739.

SHADOZ. 2023. SHADOZ Data Archive [Dataset], https://tropo.gsfc.nasa.gov/shadoz/Archive.html (last accessed 01/06/2022).

Sitch, S., Cox, P.M., Collins, W.J., et al. 2007. Indirect radiative forcing of climate change through ozone effects on the land-carbon sink. *Nature*, **448**, 791-794, doi: 10.1038/nature06059.

Sofieva, V.F., Tamminen, J., Kyrölä, E., et al. 2014. A novel tropopause-related climatology of ozone profiles. *Atmospheric Chemistry and Physics*, **14**, 283–299, doi:10.5194/acp-14-283-2014.

Stevenson, D.S., Young, P.J., Naik, V., et al. 2013. Tropospheric ozone changes, radiative forcing and attribution to emissions in the Atmospheric Chemistry and Climate Model Intercomparison Project (ACCMIP), *Atmospheric Chemistry and Physics*, **13**, 3063- 3085, doi: 10.5194/acp-13-3063-2013.

Szopa, S., V. Naik, B. Adhikary, P. Artaxo, T. Berntsen, W.D. Collins, S. Fuzzi, L. Gallardo, A. Kiendler-Scharr, Z. Klimont, H. Liao, N. Unger, and P. Zanis.: Short-Lived Climate Forcers. In Climate Change 2021: The Physical Science Basis. Contribution of Working Group I to the Sixth Assessment Report of the Intergovernmental Panel on Climate Change, edited by Masson-Delmotte, V., P. Zhai, A. Pirani, S.L. Connors, C. Péan, S. Berger, N. Caud, Y. Chen, L. Goldfarb, M.I. Gomis, M. Huang, K. Leitzell, E. Lonnoy, J.B.R. Matthews, T.K. Maycock, T. Waterfield, O. Yelekçi, R. Yu, and B. Zhou., Cambridge University Press, Cambridge, United Kingdom and New York, NY, USA, pp. 817–922, doi:10.1017/9781009157896.008, 2021.

TOMCAT. 2023. TOMCAT Simulations [Dataset], https://homepages.see.leeds.ac.uk/~earrjpo/to3re/tomcat/ (last accessed 23/01/2023).

van der Werf, G. R., Randerson, J. T., Giglio, L., et al. 2017. Global fire emissions estimates during 1997–2016. *Earth System Science Data*, **9**, 697–720, doi:10.5194/essd-9-697-2017.

Wespes, C., Hurtmans, D., Clerbaux, C., Boynard, A., and Coheur, P.-F.: Decrease in tropospheric O_3 levels in the Northern Hemisphere observed by IASI, Atmos. Chem. Phys., 18, 6867–6885, https://doi.org/10.5194/acp-18-6867-2018, 2018.

Formatted: Space Before: 6 pt

WMO, Meteorology—A three-dimensional science, World Meteorological Organisation, Bulletin 6, (Oct), 134–138, 1957.

Worden, H.M., Bowman, K.W., Worden, J.R., et al. 2008. Satellite measurements of the clear-sky greenhouse effect from tropospheric ozone. *Nature Geoscience*, 1, 305-308, doi: doi.org/10.1038/ngeo182.

Worden, H.M., Bowman, K.W., Kulawik, S.S., et al. 2011. Sensitivity of outgoing longwave radiative flux to the global vertical distribution of ozone characterized by instantaneous radiative kernels from Aura-TES. *Journal of Geophysical Research: Atmospheres*, 116 (D14115), doi:10.1029/2010JD015101.

WOUDC. 2023. Data Search/Download [Dataset], https://woudc.org/data/explore.php (last accessed 01/06/2022).

Young, P.J., Archibald, A.T., Bowman, K.W., et al. 2013. Pre-industrial to end 21st century projections of tropospheric ozone from the Atmospheric Chemistry and Climate Model Intercomparison Project (ACCMIP). *Atmospheric Chemistry and Physics*, **13**, 2063-2090, doi: 10.5194/acp-13-2063-2013.

Ziemke, J.R., Douglass, A.R., Oman, L.D., Strahan, S.E. and Duncan, B.N.: Tropospheric ozone variability in the tropics from ENSO to MJO and shorter timescales. Atmospheric Chemistry and Physics, **15** (14), 8037-8049, doi: 10.5194/acp-15-8037-2015, 2015.

Figures and Tables:

Dataset	**TCO_3 (DU)**	**TO_3RE (W/m²)**	**NTO_3RE (W/m²/DU)**	**TO_3RE Trend (%/yr)**	**TO_3RE CoV (%)**	**$DOFS_{trop}$**	**$DOFS_{utls}$**
FORLI	32.6	1.23	37.8	-0.64 (-0.99, -0.28; p = 0.00) -0.21 (-0.66, 0.23; p = 0.35)*	2.5 (1.2)*	1.1	1.2
SOFRID	29.9	1.21	40.4	-0.01 (-0.14, 0.12; p = 0.94)	1.1	0.9	1.0
IMS	29.8	1.21	40.6	-0.13 (-0.36, 0.10; p = 0.25)	1.1	1.2	1.0
TC-CLT	30.7	1.26	41	-0.05 (-0.40, 0.30; p = 0.78)	1.5	[redacted]	[redacted]
TC-EMS	30.6	1.25	40.8	-0.23 (-0.59, 0.13; p = 0.20)	1.7	[redacted]	[redacted]
TC-MET	30.1	1.27	41	0.26 (0.13, 0.39; p = 0.00)	0.9	[redacted]	[redacted]

Table 1: Summary statistics of the satellite and TOMCAT TCO_3, TO_3RE and NTO_3RE global average (2008-2017) metrics and the corresponding linear trends and covariance of variation (CoV) from **Figures 1-3**. TC-CTL, TC-EMS and TC-MET represent the control, fixed emissions and fixed meteorology runs, respectively. The global average (2008) degrees of freedom of signal (DOFS) for the IASI products are shown for the troposphere (approximately the surface to 200 hPa) and the upper troposphere – lower stratosphere (UTLS – approximately 400-100 hPa). * represents the IASI-FORLI trends for 2011-2017.

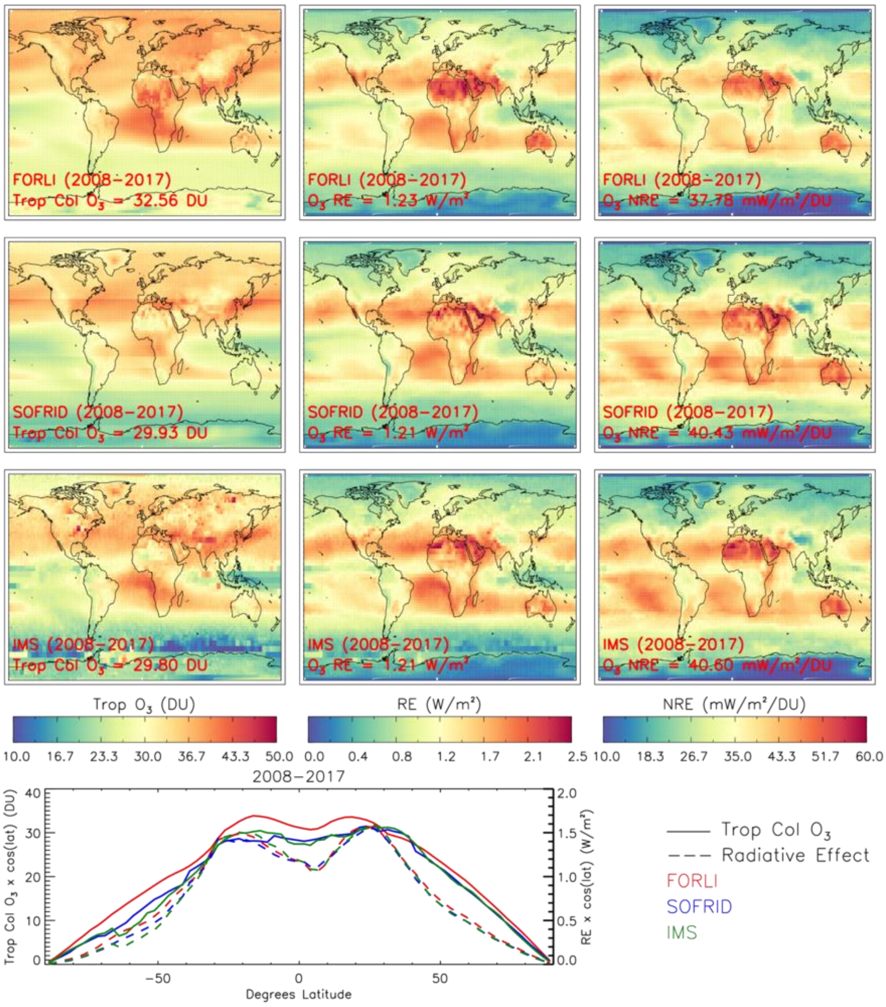

Figure 1: *Tropospheric column O_3 (TCO_3, DU), tropospheric O_3 radiative effect (TO_3RE, W/m^2) and normalised TO_3RE (NTO_3RE, $mW/m^2/DU$) averaged for 2008 to 2017 for IASI-FORLI (top row), IASI-SOFRID (middle row) and IASI-IMS (bottom row). Zonal averages of TCO_3 (DU, solid lines) and TO_3RE (W/m^2, dashed lines), both weighted by cosine of latitude, is shown in the bottom panel from all the IASI instruments.*

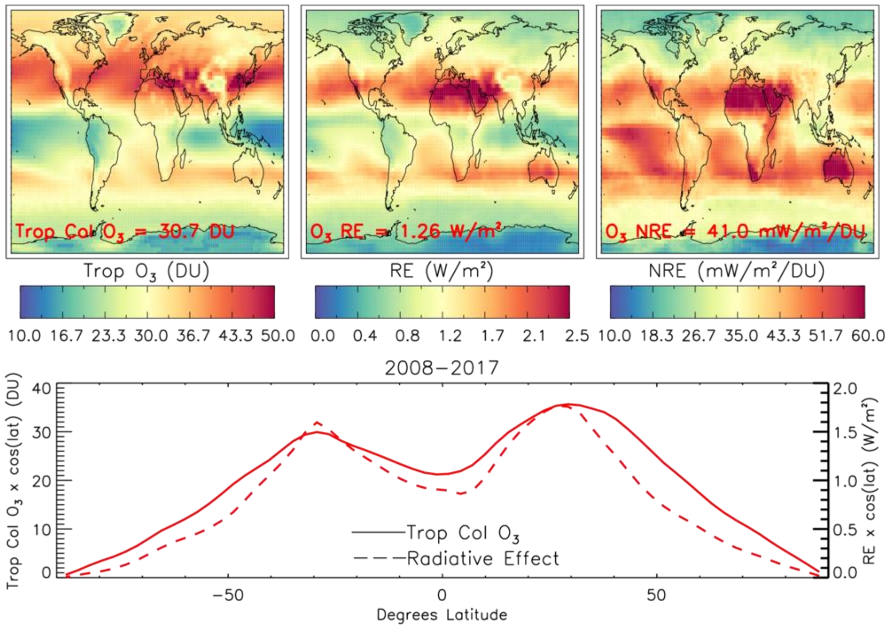

Figure 2: *TCO_3 (DU), TO_3RE (W/m^2) and NTO_3RE ($mW/m^2/DU$) averaged for 2008 to 2017 for TOMCAT. Zonal averages of TCO_3 (DU, solid lines) and TO_3RE (W/m^2, dashed lines), both weighted by cosine of latitude, is shown in the bottom panel from TOMCAT.*

Formatted: Space After: 18 pt, Line spacing: single

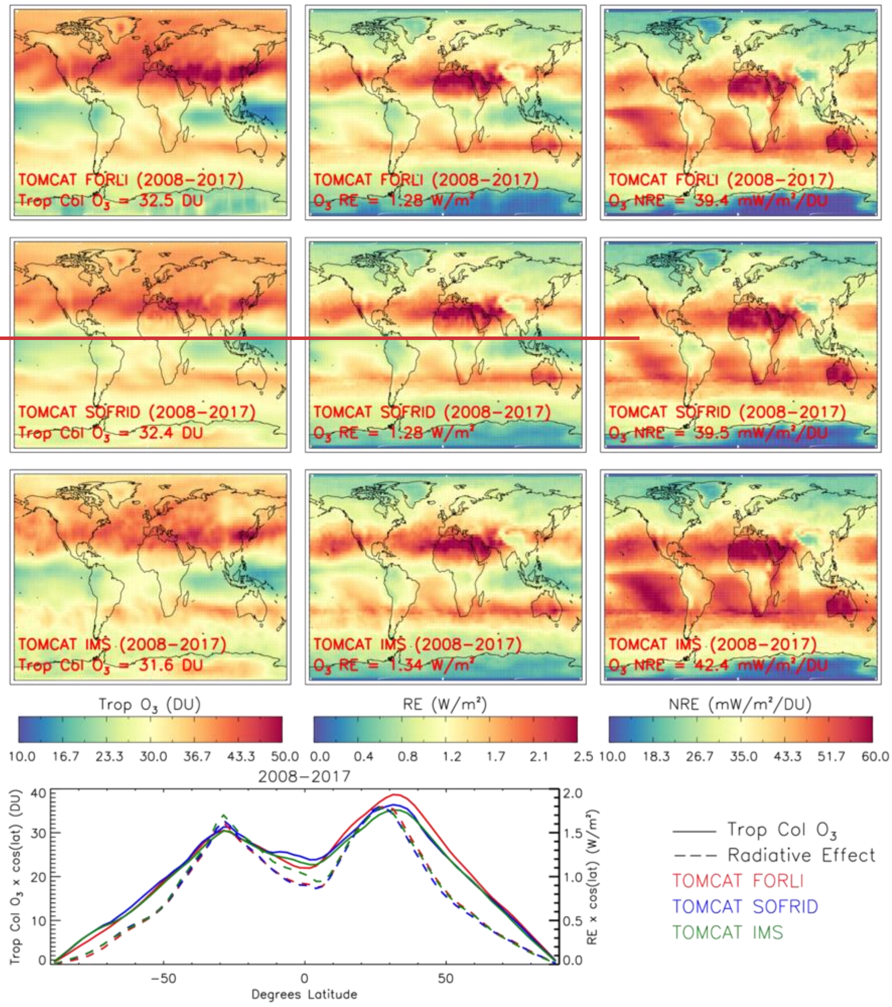

~~**Figure 2**: *TCO_3 (DU), TO_3RE (W/m^2) and NTO_3RE (mW/m^2/DU) averaged for 2008 to 2017 for TOMCAT with the averaging kernels (AKs) applied from IASI-FORLI (top row), IASI-SOFRID (middle row) and IASI-IMS (bottom row). Zonal averages of TCO_3 (DU, solid lines) and TO_3RE (W/m^2, dashed lines), both weighted by cosine of latitude, is shown in the bottom panel from all the IASI instruments.*~~

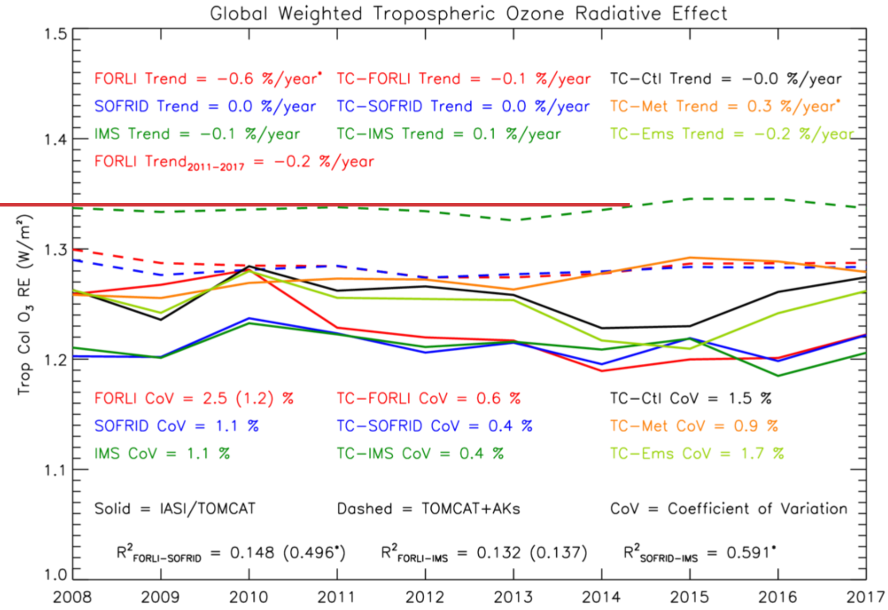

~~**Figure 3**: *Annual global mean time-series of TO_3RE (W/m^2), between 2008 and 2017, for IASI-FORLI (red-solid), IASI-SOFRID (blue-solid) and IASI-IMS (green-solid). TOMCAT with the IASI-FORLI (red-dashed), IASI-SOFRID (blue-dashed) and IASI-IMS (green-dashed) AKs applied, original TOMCAT simulation (black-solid), TOMCAT with fixed emissions (lime-solid) and TOMCAT with fixed meteorology (orange-solid) are also shown. The linear trend (%/year) is shown as well as the percentage coefficient of variation (CoV). The correlation between IASI time-series are shown by the R^2 values. Significant linear trends and correlations in the TO_3RE are shown by an *. TC represents TOMCAT. The IASI-FORLI trend for 2011 to 2017 is also shown as well as the CoV and R^2 in brackets in addition to the statistical metrics over the full time period due to record inhomogeneities prior to 2011 (Boynard et al., 2018).*~~

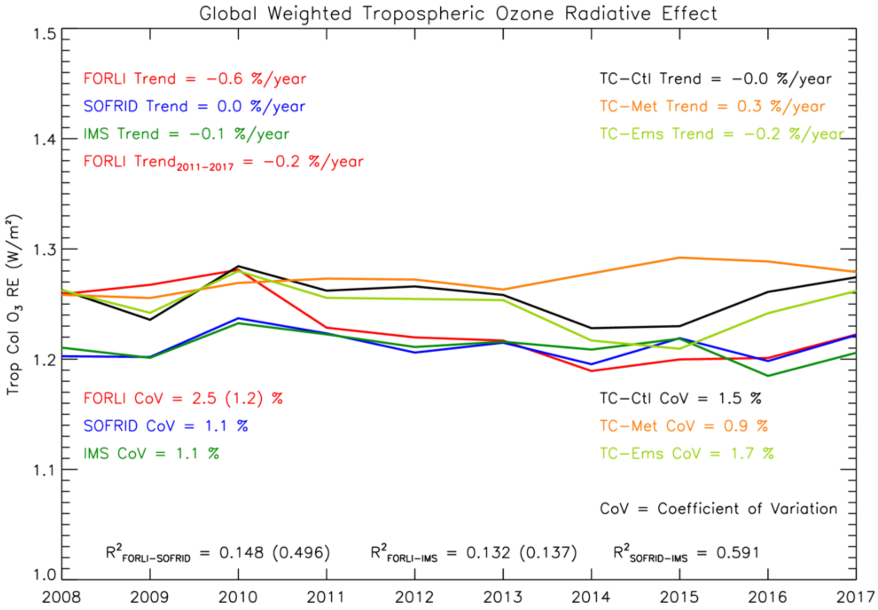

Figure 3: *Annual global mean time-series of TO_3RE (W/m^2), between 2008 and 2017, for IASI-FORLI (red-solid), IASI-SOFRID (blue-solid) and IASI-IMS (green-solid). TOMCAT simulation (black-solid), TOMCAT with fixed emissions (lime-solid) and TOMCAT with fixed meteorology (orange-solid) are also shown. The linear trend (%/year) is shown as well as the percentage coefficient of variation (CoV). The correlation between IASI time-series are shown by the R^2 values. TC represents TOMCAT. The IASI-FORLI trend for 2011 to 2017 is also shown as well as the CoV and R^2 in brackets in addition to the statistical metrics over the full time period due to record inhomogeneities prior to 2011 (Boynard et al., 2018).*

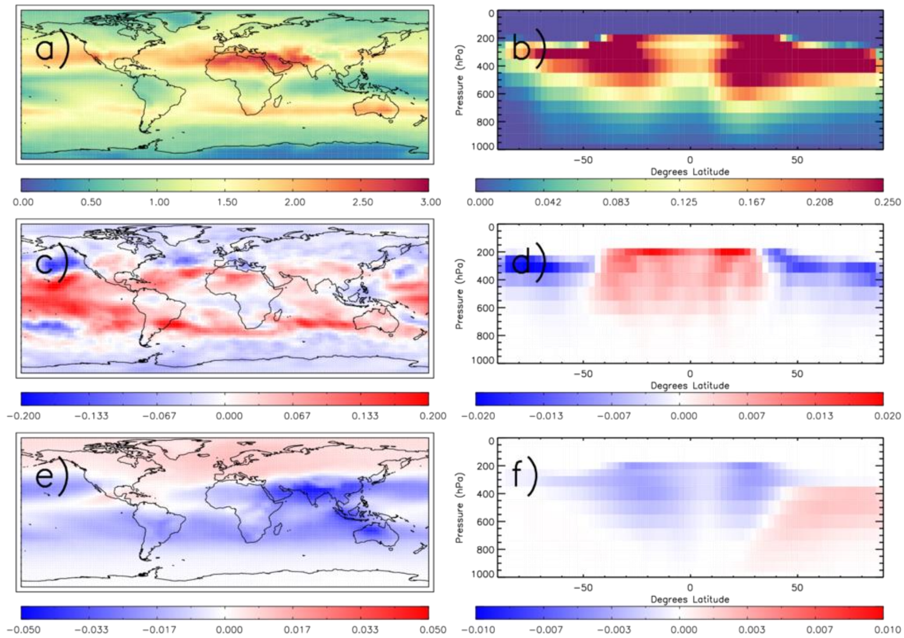

Figure 4: a) *TOMCAT control run* TO_3RE *(W/m*^{2}*), b) TOMCAT control run zonal average grid box* O_3 *radiative effect (W/m*^{2}*), c) TOMCAT fixed meteorology – TOMCAT control* TO_3RE *difference (W/m*^{2}*), d) TOMCAT fixed meteorology – TOMCAT control zonal average grid box* O_3 *radiative effect difference (W/m*^{2}*), e) TOMCAT fixed emissions – TOMCAT control* TO_3RE *difference (W/m*^{2}*), f) TOMCAT fixed emissions – TOMCAT control zonal average grid box* O_3 *radiative effect difference (W/m*^{2}*).*